PII: S0955-2219(98)00154-X
Printed in Great Britain. All rights reserved
0955-2219/98/$—see front matter

In-situ Fabrication of Ceramic/Metal Nanocomposites by Reduction Reaction in Barium Titanate–Metal Oxide Systems

Hae Jin Hwang,[a]* Motohiro Toriyama,[a] Tohru Sekino[b] and Koichi Niihara[b]

[a]National Industrial Research Institute of Nagoya, Nagoya 462-8510, Japan
[b]The Institute of Scientific and Industrial Research, Osaka University, Osaka 567-0047, Japan

(Received 6 February 1998; revised version received 10 June 1998; accepted 16 June 1998)

Abstract

Novel ceramic/metal nanocomposites were prepared by in-situ reduction method in $BaTiO_3/NiO$, $BaTiO_3/WO_3$ and $BaTiO_3/MoO_3$ systems. The fabrication processes and the phase stability of these metal and metal oxides were studied using X-ray diffraction analysis and thermodynamic consideration. For $BaTiO_3/NiO$ system, NiO was entirely reduced at 500°C for several hours and dense $BaTiO_3/Ni$ nanocomposites were obtained without additional reaction phases. However, it was confirmed that a small amount of Ni^{2+} was dissolved in the $BaTiO_3$ lattice. In the $BaTiO_3/WO_3$ system, in parallel with the reduction of WO_3, $BaTiO_3$ reacted with WO_3 or WO_2 to produce $BaWO_4$. $BaTiO_3/W$ composite powder having no reaction products was difficult to fabricate by in-situ reduction process. On the other hand, $BaTiO_3/W$ composite could be obtained from $BaTiO_3$ and W powder mixture when sintering below 1200°C. In contrast, the fabrication of $BaTiO_3/Mo$ composite was successfully achieved after reducing $BaTiO_3/MoO_3$ powder mixture at 800°C. *© 1998 Elsevier Science Limited. All rights reserved*

1 Introduction

Because of the peculiar electrical characteristics originating from the perovskite type crystal structure, barium titanate ($BaTiO_3$) and its related compounds have been technologically important electroceramics widely used as high-capacitance capacitors, PTC thermistors and so on. With the development of the electronic industries, high-performance ferroelectric devices exhibiting specific functions and good reliability are increasingly required. Many investigators have tried to modify the microstructure and properties of these compounds by different means to achieve stable electronic devices with satisfactory operational capacity.[1–4] Previously, Newnham *et al*.[5] has stated that single phase materials could no longer satisfy the demand for the high-performance and multifunctional ferroelectric devices, and they have proposed novel piezoelectrics-based composites composed of two or more phases.

In the past few years, the authors have proposed ceramic nanocomposite, and have reported high strength and toughness ferroelectrics-based nanocomposite such as $BaTiO_3/SiC$[6] and PZT/Ag.[7,8] Of the nanocomposites, metallic particle-dispersed piezoelectric ceramics showed unique properties; relative dielectric constant increased with increasing a volume fraction of a metal particle. The metal particle relieved transformation-induced internal stress of ferroelectric ceramics, and ferroelectric-to-paraelectric phase transition temperature, the Curie temperature could be controlled in PZT/Ag composite system. Both fracture toughness, K_{IC} and fracture strength was enhanced, which was considered to result from the increased fracture energy due to the ductile behavior of a metal particle.[9,10] In addition, it would be expected that the metal particle can modify domain structure, which are frequently observed in the ferroelectric ceramics, and also domain wall movement because an electric field can be modified around the metal particle.

The present study is concerned with establishing the fabrication processes of $BaTiO_3$/metal composites. To fabricate the metal particle-dispersed ferroelectrics, the matrix should be not reacted with

*To whom correspondence should be addressed. Fax: +81-52-916-2802; e-mail: hwang15@nirin.go.jp

the metal particle during the fabrication processing. However, ferroelectric ceramics like $BaTiO_3$ easily react with metal and oxides to produce unwanted reaction products. The focus was placed on reviewing the phase stability of metal and metal oxides mainly using X-ray diffraction analysis and thermodynamic considerations. Various $BaTiO_3$-based composites containing fine metal particles such as Ni, W, Mo were fabricated by in-situ reduction method.

2 Experimental Procedure

In-situ fabrication of $BaTiO_3$-based composites ceramics containing fine metal particles were performed by the hydrogen reduction of $BaTiO_3$ and metal oxide powder mixtures and subsequent pressureless sintering or hot-pressing in an inert atmosphere.

Chemically pure $BaTiO_3$ (BT01, Sakai Chemical Co. Ltd., Osaka, Japan), nickel monoxide (NiO), tungsten trioxide (WO_3) and molybdenum trioxide (MoO_3) were used as starting materials. $BaTiO_3$ and metal oxide powder was wet-milled in a polyethylene jar using ethyl alcohol and ZrO_2 balls for 24 h. The mixed slurry was dried and dry-milled, and then sieved through a 320 μm mesh screen. The mixed powders of $BaTiO_3$/metal oxide were reduced in about 99% H_2 atmosphere at 500 to 800°C and subsequently hot-pressed at 1100 to 1300°C at 30 MPa for 1 h in an argon atmosphere. Some specimens were pressurelessly sintered at 1200 to 1350°C for 2 h in the same atmosphere.

For phase characterization, X-ray diffraction pattern (50 kV–150 mA, RU-200B, Rigaku Co. Ltd., Japan) was obtained at 25°C. The diffraction pattern was taken using Ni-filtered CuK_α radiation. The lattice constant was calculated by using reflections from (200), (002), (112), (211), (202), (220), (212) and (221) planes that are sensitive to the crystal structure change of the perovskite crystal structure. Pure silicon powder (99·999%) was used as internal standard material. The temperature dependence of crystal structure was investigated using a high temperature X-ray diffractometry (35 kV–25 mA, Automated Powder Diffraction APD1700HL, Phillips Co., Ltd., USA). X-ray diffraction data were collected on heating at 25°C to 150°C. The bulk density was determined by the Archimedes method in water. The microstructures of the sintered specimens were observed with a scanning electron microscope (SEM, 20 kV, S-5000, Hitachi Co., Ltd., Japan) and a transmission electron microscope (TEM, 200 kV, H-8100, Hitachi Co., Ltd., Japan).

3 Results and Discussion

3.1 Thermodynamic considerations

Consider the reaction equilibrium between a solid metal M, its metal oxide MO and oxygen gas at temperature T and pressure P. The standard Gibbs free energy change, ΔG^o, is written as follows;

$$M(s)+1/2O_2(g)= MO(s) \quad (1)$$

$$\Delta G^o = -RT \ln K \quad (2)$$

where equilibrium constant K is equal to $1(pO_2)^{1/2}$. As ΔG^o is a function only of temperature, then K is a function only of temperature, and therefore at any fixed temperature the establishment of reaction equilibrium occurs at a unique value of pO_2, i.e. equilibrium oxygen partial pressure pO_2 (eq, T). If, at any temperature T, the actual oxygen partial pressure in a closed M–MO–O_2 system is greater than pO_2 (eq, T), then spontaneous oxidation of the metal will occur, thus consuming oxygen and decreasing the oxygen partial pressure in the gas phase. When the actual oxygen pressure has thus been lowered to pO_2(eq, T), then provided that both solid phases are still present, the oxidation reaction ceases and equilibrium prevails. Conversely, if the oxygen partial pressure was less than pO_2 (eq, T), then spontaneous reduction of the oxide would occur until pO_2 (eq, T) was reached.

Figure 1 shows the ΔG^o versus temperature relationships (Ellingham diagram) for various

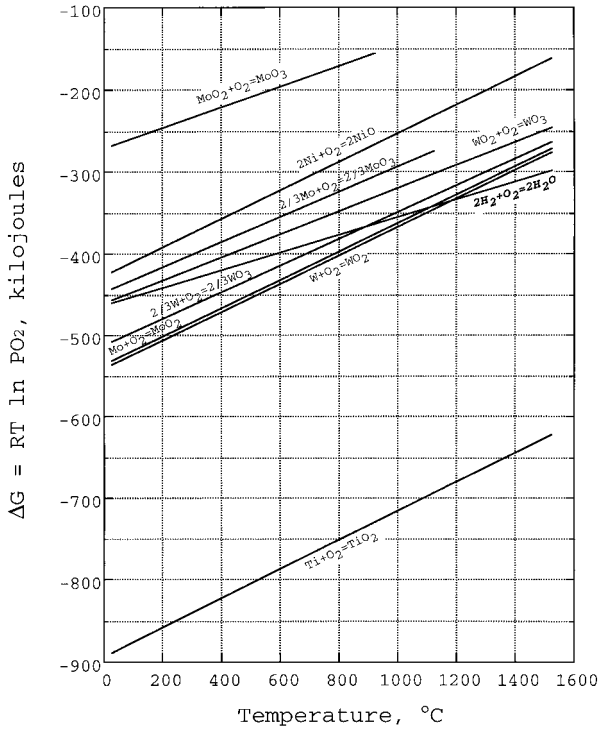

Fig. 1. ΔG^o versus temperature relationships for various metal–metal oxide systems.

metal–metal oxide systems that will be dealt with in the present study. In comparing with any oxides illustrated in Fig. 1, TiO_2 is extremely difficult to reduce unless the reduction is carried out at high temperature and the oxygen partial pressure pO_2 is sufficiently lower than the equilibrium value. On the other hand, NiO is expected to be easily reduced even at low temperatures and high oxygen partial pressures.

As the reduction process is carried out using an H_2–H_2O gas mixture as the reducing agents, as in the present study, the reduction reaction can be expressed as follows

$$MO(s) + H_2(g) = M(s) + H_2O(g) \qquad (3)$$

If the ΔG_3^o of reaction (3) is positive, the reduction reaction is not likely to go on, and while the ΔG_3^o is negative, the metal oxide MO will be reduced spontaneously. As a matter of convenience, reaction (3) can be divided into the two following equations.

$$2M(s) + O_2(g) = 2MO \qquad (4)$$

$$2H_2(g) + O_2(g) = 2H_2O(g) \qquad (5)$$

for which $\Delta G_3^o = 1/2\left(\Delta G_5^o - \Delta G_4^o\right)$. The estimate of the sign for reaction (3), i.e. whether the reduction reaction proceeds or not, is determined by the difference between the ΔG_5^o and ΔG_4^o. The Ellingham line for reaction, $2H_2(g) + O_2(g) = 2H_2O(g)$ ($pH_2/pH_2O = 1$) is also included in Fig. 1. If the Ellingham line of any metal-metal oxide system is higher than that of reaction (5), reduction is thermodynamically possible.

Figure 2 shows the variation of log pO_2(eq, T) with $1/T$ for various metal and metal oxides systems in the present study. Also log $pO_2 - 1/T$ relationships are shown for reaction (5) at various pH_2/pH_2O value. All points on these lines represent the oxygen pressure pO_2(eq, T) required for equilibrium between metal(s), metal oxide(s) and oxygen(g) at the particular temperature T. If $pO_2 > pO_2$(eq, T), i.e. above each line, the metal oxide phase is stable, and if $pO_2 < pO_2$(eq, T), i.e. below the lines the metal is stable. As mentioned earlier, at the particular pH_2/pH_2O, the temperature at which the reduction proceeds can be determined from the interception between two pO_2(eq, T) $- 1/T$ lines.

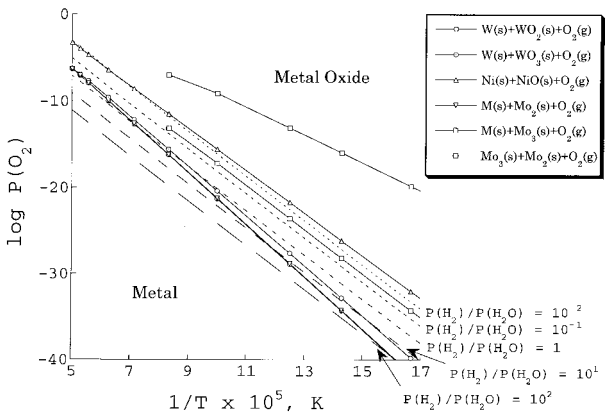

Fig. 2. Temperature dependence of oxygen partial pressure required for maintenance of equilibrium $M(s)+O_2(g) = MO_2(s)$.

3.2 Barium titanate–nickel oxide system

Table 1 shows the relative density for $BaTiO_3$/Ni composites hot-pressed or pressureless-sintered at various temperatures. In all cases, almost fully-densified $BaTiO_3$/Ni composites could be obtained when sintered above 1200°C and 1250°C by hot-pressing and pressureless sintering methods, respectively. For the hot-pressed specimens, the relative density increased with the sintering temperature and decreased with Ni content. In the case of pressureless-sintered $BaTiO_3$/Ni composites, although the relative density decreased compared with those of the hot-pressed specimens, high density over 98% of theoretical density was achieved when sintering above 1250°C for 2 h.

As illustrated in Fig. 2, if the pH_2/pH_2O is approximately higher than 10^{-2} to 10^{-3}, from a thermodynamic point of view, NiO is reduced to Ni metal in the entire temperature range. If the pH_2/pH_2O used in the present study is assumed to be approximately 10^2 (the purity of H_2 gas is approximately 99%), it is not surprising that the reduction of NiO occurs even at low temperatures. The X-ray diffraction patterns for $BaTiO_3$/NiO system are shown in Fig. 3. Neither NiO nor other unwanted reaction compounds were detectable after reducing the powder mixture at 500°C for 2 h, as is evident in Fig. 3(a) and (b). Following the reduction of NiO, dense $BaTiO_3$/Ni composites were successfully fabricated *in situ* by sintering at 1300°C for 2 h [see Fig. 3(c)–(e)]. $BaTiO_3$/Ni

Table 1. Relative densities for $BaTiO_3$/Ni composites

Ni content (vol%)	*Hot-pressed*			*Pressureless sintered*	
	1100°C	*1200°C*	*1300°C*	*1250°C*	*1300°C*
0	98·52	99·70	99·78	96·10	97·42
3	97·34	99·95	99·82	98·56	99·08
5	96·78	99·97	99·82	98·85	99·27
10	95·91	98·33	99·95	98·83	98·86
20	—	—	—	98·62	—
30	—	—	—	99·42	—
40	—	—	—	97·41	—
50	—	—	—	98·46	

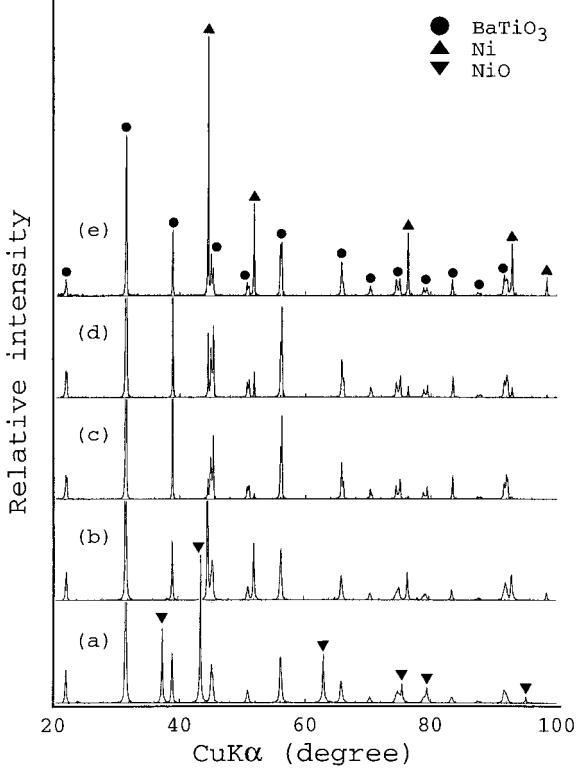

Fig. 3. The X-ray diffraction patterns for $BaTiO_3$/Ni systems; (a) $BaTiO_3$/NiO starting powder for $BaTiO_3$/40 vol% Ni, (b) $BaTiO_3$/40 vol% Ni composite powder after reducing powder (a) at 500°C for 2 h, (c) $BaTiO_3$/3 vol% Ni composite reduced at 500°C in H_2 and sintered at 1300°C for 2 h in Ar, (d) $BaTiO_3$/20 vol% NI composite fabricated by the same condition of (c), and (e) $BaTiO_3$/40 vol% Ni composite fabricated by the same conditions of (c).

composites consisted only of $BaTiO_3$ and Ni metal and thus the incorporation of the Ni particle into $BaTiO_3$ matrix gave no additional phases, i.e. reaction compounds between $BaTiO_3$ and Ni or NiO. The crystal structure of the $BaTiO_3$ matrix of both hot-pressed and pressureless-sintered $BaTiO_3$/Ni composites was tetragonal regardless of the Ni content and sintering temperature. Some $BaTiO_3$/Ni composites that contain high volume percent of Ni and were sintered below 1200°C were, however, not tetragonal, but pseudo-cubic, judging by the split of tetragonal characteristic peaks at around $2\theta = 45°$.

Here, notice the diffraction peaks of (002) and (200) planes of $BaTiO_3$/Ni composites between $2\theta = 44{\cdot}8°$ and $2\theta = 45{\cdot}6°$ in Fig. 3(c)–(e). The ratio of the two intensities, $I_{(002)}/I_{(200)}$ in $BaTiO_3$/Ni composites sintered at 1250°C and 1300°C is summarized in Table 2. The typical value of the ratio $I_{(002)}/I_{(200)}$ in pure $BaTiO_3$ ceramics is known to be about 0·32 which means that domains are randomly oriented.[11] In the present study, $I_{(002)}/I_{(200)}$ increased gradually with increasing Ni content regardless of the sintering temperature, and when the Ni content is equivalent, $I_{(002)}/I_{(200)}$ of composites sintered at 1300°C is larger than those

Table 2. $I_{(002)}/I_{(200)}$ change with the Ni content for $BaTiO_3$/Ni composites sintered at 1250°C and 1300°C for 2 h in Ar atmosphere

Ni content (vol%)	$I_{(002)}/I_{(200)}$	
	1250°C	*1300°C*
0	0·32	0·32
3	0·58	0·71
5	0·57	0·70
10	0·62	0·77
20	0·74	0·79
30	0·85	0·95
40	1·00	1·15
50	1·11	—

of the composites sintered at 1250°C. Generally, the increase in $I_{(002)}/I_{(200)}$ occurs in piezoelectric ceramics such as $BaTiO_3$ and $Pb(Zr,Ti)O_3$ when the 90° domains are aligned along the poling direction, i.e. suggesting the occurrence of domain reorientation due to the domain switching under an electric field or mechanical stress.[11] However, as the X-ray beam, in the present study, was scanned on the pristine (annealed) surface with no electrical or mechanical field the increase in $I_{(002)}/I_{(200)}$ is caused not by the 90° domain reorientation, but by other reasons, which as will be discussed in the next paragraphs.

From the microstructure evaluation by SEM and TEM (Fig. 4), the reduced Ni particles were dispersed within the $BaTiO_3$ matrix grains and at grain boundaries. When Ni particles are dispersed within the matrix grains, $BaTiO_3$ lattices may experience complex stresses, just as the same reason as the foreign ions substituted for $BaTiO_3$ lattice do, and thus a change in domain structure appears to results in the increase in the intensity ratio $I_{(002)}/I_{(200)}$.

The presence of the foreign ions in the $BaTiO_3$ lattice can result in strong restriction of motion of domain boundaries, which is due to lattice strain at the sites of foreign ions.[12,13] Therefore, the observed $I_{(002)}/I_{(200)}$ variation with Ni content may be attributable to the substitution of Ni ions into the $BaTiO_3$ lattice. Examination on lattice constants variation with the Ni content (Fig. 5) indicates that, with increasing Ni content up to 30 vol%, the *c*-axis lattice constant decreased and, by contrast, *a*-axis increased as the Ni content increased. Thereafter, both *a*-axis or *c*-axis were nearly saturated and no remarkable change was observed. These observed increase in *a*-axis and decrease in *c*-axis results in the decrease in tetragonality. Lattice constants and tetragonality variation with increasing Ni content must be caused by the substitution of Ni^{2+} for Ti^{4+} of the perovskite crystal structure. Figure 6 shows the relationship between the unit cell volume and Ni content for the

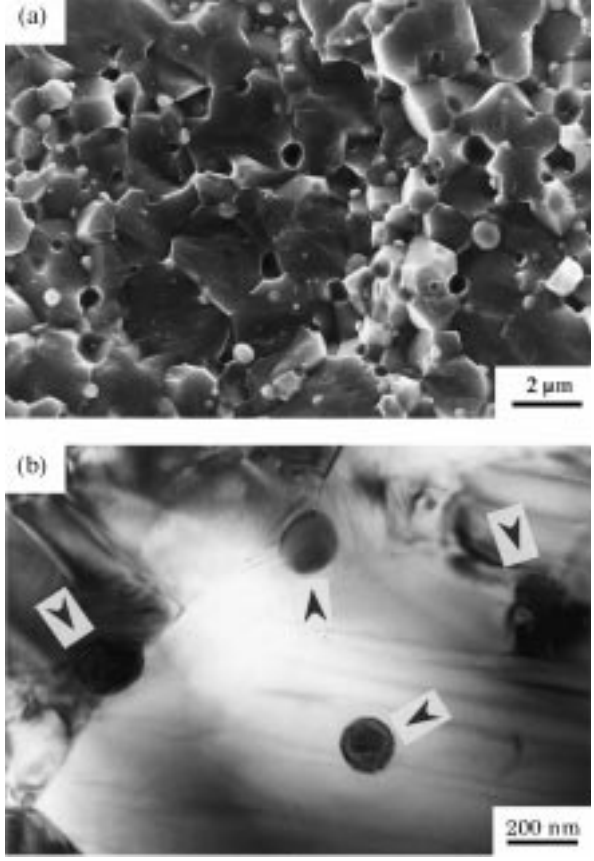

Fig. 4. SEM and TEM photographs for $BaTiO_3$/5 vol% Ni composite hot-pressed at 1300°C for 1 h; (a) SEM photograph showing fracture surface and (b) TEM photograph showing intra- and intergranular Ni. Allows indicate Ni particles.

same specimens as in Fig. 5. The unit cell volume is expanded with Ni content. The effective ionic radii of Ti^{4+} in perovskite crystal structure are 0·61 Å. That of the Ni^{2+} is 0·70 Å.[14] Therefore, the substitution for Ti^{4+} site leads to an expansion of the unit cell. From the results of Figs 5 and 6, it is concluded that a small amount of Ni^{2+} was dissolved into the $BaTiO_3$ lattice and substituted mainly for Ti^{4+} sites.

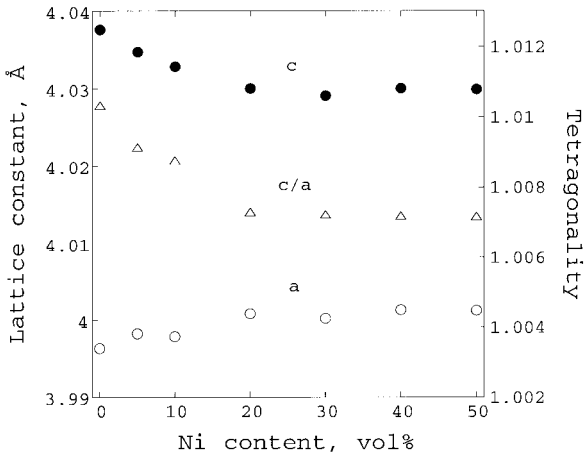

Fig. 5. Lattice constants and tetragonality variation with Ni content for $BaTiO_3$/Ni nanocomposites sintered at 1300°C for 2 h.

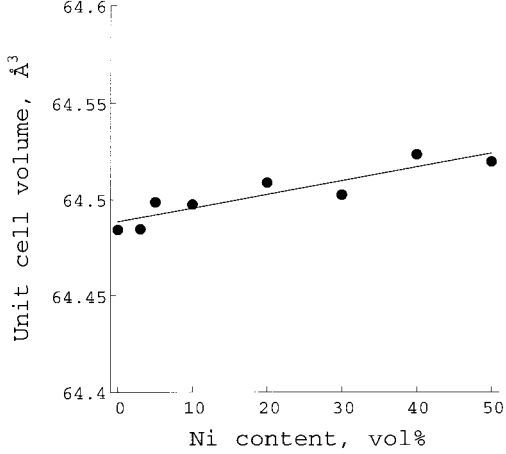

Fig. 6. Unit cell volume variation with Ni content for $BaTiO_3$/Ni nanocomposites sintered at 1300°C for 2 h.

Figure 7 shows the temperature dependence of the X-ray diffraction pattern for the $BaTiO_3$/20 vol% Ni composite sintered at 1300°C. The tetragonal to cubic phase transformation temperature can be roughly estimated from the split of (002) and (200) diffraction lines. In Fig. 6, as is obvious that with increasing temperature the split of (200) and (002) move closer together and finally coalesces into a single peak. The split was clearly observed up to 90°C, became ambiguous at 95°C, and thereafter coalesced into a single peak above 100°C. Therefore, the tetragonal to cubic transformation probably occurred at around 100°C that is lower than transformation temperature of monolithic $BaTiO_3$ ceramics sintered at the same temperature under an inert atmosphere, i.e. 110°C. From the X-ray diffraction patterns in Fig. 6, it is clear that a small amount of Ni is dissolved into the matrix lattice.

3.3 Barium titanate–tungsten oxide system

As is evident from the Ellingham lines related to W, WO_2 and WO_3 (Fig. 1), log pO_2 for WO_3

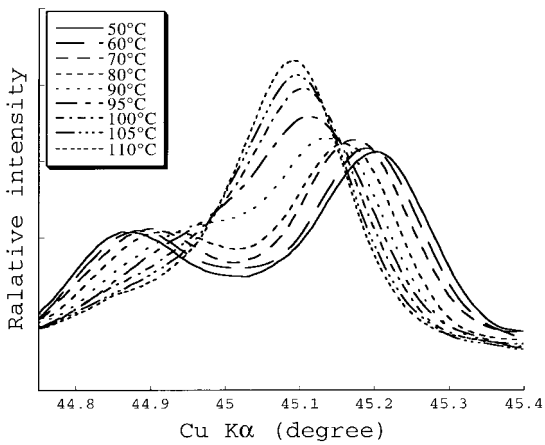

Fig. 7. Temperature dependence of X-ray diffraction profiles for $BaTiO_3$/20 vol% Ni composite sintered at 1300°C.

intercepts pH_2/pH_2O curves at about 550°C and 850°C for $pH_2/pH_2O = 10^1$ and $pH_2/pH_2O = 1$, respectively. As pH_2/pH_2O, in the present study, is at least higher than 10^2 and the known reduction path is $WO_3 \rightarrow WO_{2.90}$ or $WO_{2.72} \rightarrow WO_2 \rightarrow W$, WO_3 is thermodynamically favorable below 550°C. Nevertheless, the reduction reaction did not proceed below 800°C. Figure 8 shows the X-ray diffraction profiles for $BaTiO_3$/5 vol% W composite powder held at 600, 700 and 800°C for 2 h in H_2 atmosphere. Also shown is the X-ray diffraction pattern for a $BaTiO_3$/20 vol% W composite hot-pressed at 1200°C for 1 h. Specimen (d) was prepared by sintering $BaTiO_3$ and tungsten metal mixture. When reduced at 600°C, the color of the $BaTiO_3/WO_3$ powder changed from yellow to deep blue, indicating the presence of $WO_{2.90}$. Also from the X-ray analysis the existence of $WO_{2.90}$ was confirmed, but there was no $WO_{2.72}$ phase. These results are in good agreement with the sequence of reduction for the W–O system.[16] As the reduction temperature increases, it is suggested that the reaction between $BaTiO_3$ and $WO_{2.90}$ or WO_2 coincide with the reduction of $WO_{2.90}$. Rather than reduced metal tungsten peaks, $BaWO_4$ phase, i.e. reaction compound between $BaTiO_3$ and $WO_{2.90}$ or WO_2 was more clearly observed. From the facts that no WO_2 peaks were observed over the entire temperature range and the relative intensities of $BaWO_4$ phase is high compared with those of the reduced W, it was concluded that the reaction of $BaTiO_3 + WO_{2.90}$ or $WO_2 \rightarrow BaWO_4$ is extremely rapid. Although the tungsten metal peaks were first confirmed by the X-ray diffraction analysis when reduced at 800°C for 2 h, its intensities are weak compared with those of $BaWO_4$ phase. Since the reactivity between $WO_{2.90}$ and $BaTiO_3$ is even faster than the reduction of $WO_{2.90}$, it seems to be extremely difficult to reduce WO_3 completely to fabricate $BaTiO_3$/W composite by the in situ reduction method, unless the reduction is performed at lower temperatures for extended times.

On the other hand, $BaTiO_3$/20 vol% W composites containing no reaction compounds could be fabricated by a commercial method, i.e. from the mixture of $BaTiO_3$ and fine W powder [Fig. 8(d)]. $BaTiO_3$/20 vol% W composites sintered below 1200°C were composed only of $BaTiO_3$ and W. $BaWO_4$ started to appear after sintering at 1250°C for 1 h. The metal W and $BaTiO_3$ matrix might react to produce the $BaWO_4$ phase. The details of the reaction processes between $BaTiO_3$ and metal W are not clear. It is concluded, therefore, in order to fabricate $BaTiO_3$/W composites having no additional secondary phases, low temperature sintering below 1200°C is required. Alternative processes are now under investigation.

3.4 Barium titanate–molybdenum oxide system

Figure 9 shows the X-ray diffraction patterns for the $BaTiO_3/MoO_3$ composite powder exposed at

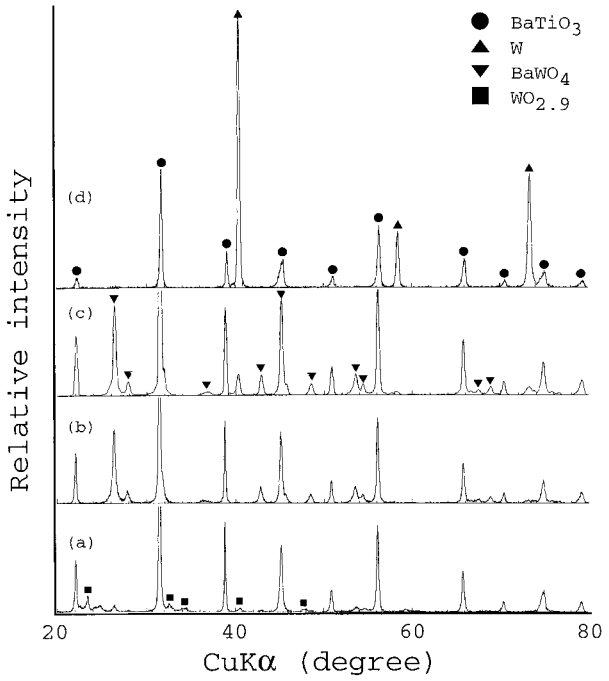

Fig. 8. The X-ray diffraction patterns showing the process of WO_3 reduction for $BaTiO_3$/5 vol% W composite powder reduced at 500°C for 2 h, (b) $BaTiO_3$/5 vol% W composite powder reduced at 700°C for 2 h, (c) $BaTiO_3$/5 vol% W composite powder reduced at 800°C for 2 h, and (d) $BaTiO_3$/20 vol% W composite hot-pressed at 1200°C for 1 h.

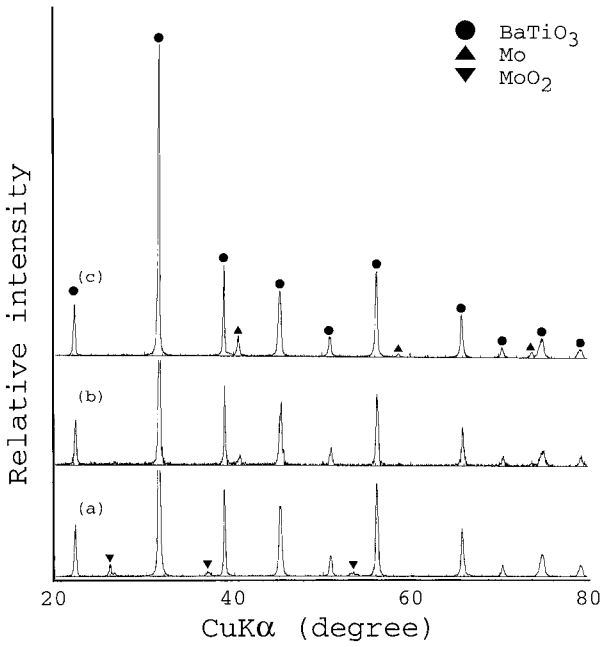

Fig. 9. The X-ray diffraction patterns showing the processes of MoO_3 reduction for $BaTiO_3$Mo system; (a) $BaTiO_3$/5 vol% W composite powder reduced at 700°C for 4 h, (b) $BaTiO_3$/5 vol% W composite powder reduced at 750°C for 4 h, and (c) $BaTiO_3$/5 vol% W composite powder reduced at 800°C for 2 h.

700°C (4 h), 750°C (4 h) and 800°C (2 h). As is evident from Fig. 9, the reduction of molybdenum trioxide is $MoO_3 \rightarrow MoO_2 \rightarrow Mo$ and there were no reaction phases between $BaTiO_3$ and MoO_3 or MoO_2 throughout all reduction processes. Please note thermodynamic data in Fig. 1. The pO_2 versus $1/T$ curve of MoO_3–MoO_2–O_2 is much higher than those of Mo–MoO_3–O_2 and Mo–MoO_2–O_2 and showing that the reduction of MoO_3 to MoO_2 is likely to occur even at lower temperatures. The rate controlling step for the reduction of molybdenum oxide is, therefore, the reduction of MoO_2 to Mo. The starting MoO_3 powder was completely reduced to MoO_2 and there were only $BaTiO_3$ and MoO_2 when reducing at 700°C and below. MoO_2 peaks disappeared completely and, at the same time, Mo peaks started to appear after reducing at 750°C for 4 h.

4 Conclusion

Novel ceramic/metal nanocomposites were fabricated by in-situ reduction from $BaTiO_3$ and various metal oxide systems, $BaTiO_3$/NiO, WO_3 and MoO_3 systems.

For $BaTiO_3$/NiO system, NiO started to be reduced at 350°C and $BaTiO_3$/Ni composites with 3 to 50 vol% Ni were successfully fabricated without additional reaction phases between $BaTiO_3$ and Ni (NiO). It was confirmed that a small amount of Ni^{2+} was dissolved into the $BaTiO_3$ matrix and, as a consequence, the lattice constants and unit cell volume were modified as Ni content increased. The Curie temperature shifted to approximately 100°C for $BaTiO_3$/20 vol% Ni. As is evident from the change in the intensity ratio of (200) to (002), the domain structure was modified by the incorporation of Ni and it was attributed to either the Ni^{2+} substitution or the incorporation of Ni particles within the $BaTiO_3$ matrix.

In $BaTiO_3/WO_3$ system, since the reaction between $BaTiO_3$ and WO_3 or WO_2 occurred in parallel with the reduction of WO_3, $BaTiO_3$/W composite powder without any kinds of reaction products is impossible to fabricate by in-situ reduction process. Alternately, $BaTiO_3$/20 vol% W composite could be obtained from $BaTiO_3$/W powder mixture when sintered at 1200°C.

As the reactivity between $BaTiO_3$ and MoO_2/MoO_3 was small, if any, at the temperature that MoO_2 could be reduced to Mo metal, the fabrication of $BaTiO_3$/Mo composite powder was successfully achieved by reducing $BaTiO_3/MoO_3$ powder at 800°C.

Acknowledgements

The authors would like to thank Mr Kazunobu Abe and Mr Masashi Aoki, Sakai Chemical Industry Co. Ltd for supplying the barium titanate powder used in the present study.

References

1. Hsieh, H. L. and Fang, T. T., Effect of green state on sintering behavior and microstructural evolution of high-purity barium titanate. *J. Am. Ceram. Soc.*, 1990, **73**, 1566–1573.
2. Becker, R. E. and Cannon, W. R., Source of water and its effect on tape casting barium titanate. *J. Am. Ceram. Soc.*, 1990, **73**, 1312–1317.
3. Ihrig, R., The phase stability of $BaTiO_3$ as a function of doped 3d elements: an experimental study. *J. Phys. C: Solid State Phys.*, 1978, **11**, 819–827.
4. Ting, C. J., Peng, C. J., Lu, H. Y. and Wu, S. T., Lanthanum–magnesium and lanthanum manganese-donor-acceptor-codoped semiconducting barium titanate. *J. Am. Ceram. Soc.*, 1990, **73**, 329–334.
5. Newnham, R. E., Skinner, D. P. and Cross, L. E., Connectivity and piezoelectric-pyroelectric composites. *Mater. Res. Bull.*, 1978, **13**, 525–536.
6. Hwang, H. J. and Niihara, K., Perovskite-type $BaTiO_3$ ceramics containing particulate SiC. *J. Mat. Sci.*, 1998, **33**, 549–558.
7. Hwang, H. J., Watari, K., Sando, M., Toriyama, M. and Niihara, K., Low temperature sintering and high strength $Pb(Zr,Ti)O_3$-matrix composites incorporating silver particles. *J. Am. Ceram. Soc.*, 1997, **80**, 791–793.
8. Hwang, H. J., Nagai, T., Ohji, T., Sando, M., Toriyama, M. and Niihara, K., Curie temperature anomaly in lead zirconate titanate/silver composites. *J. Am. Ceram. Soc.*, 1988, **81**, 709–712.
9. Tuan, W. H. and Wu, J. M., Effect of microstructure on the hardness and fracture toughness of $YBa_2Cu_3O_{-x}$/Ag composites. *J. Mater. Sci.*, 1993, **28**, 1415–1420.
10. Tuan, W. H. and Chen, W. R., Mechanical properties of alumina–zirconia–silver composites. *J. Am. Ceram. Soc.*, 1995, **78**, 465–469.
11. Mehta, K. and Virkar, A. V., Fracture mechanics in ferroelectric–ferroelastic lead zirconate titanate (Zr:Ti = 0·54:0·46) ceramics. *J. Am. Ceram. Soc.*, 1990, **73**, 567–574.
12. Arlt, G. and Neumann, R., Internal bias in ferroelectric ceramics: origin and time dependence. *Ferroelectrics*, 1988, **87**, 109–120.
13. Baxter, P., Hellicar, N. J. and Lewis, B., Effect of additives of limited solid solubility on ferroelectric properties of barium titanate ceramics. *J. Am. Ceram. Soc.*, 1959, **42**, 465–470.
14. Shannon, R. D. and Prewitt, C. T., Effective ionic radii in oxides and fluorides. *Acta Cryst.*, 1969, **B25**, 925–946.
15. Sarin, K., Morphological changes occurring during reduction of WO_3. *J. Mater. Sci.*, 1975, **10**, 593–598.
16. Phillips, B. and Chang, L. L. Y., *Trans. Metall. Soc. AIME*, 1964, **230**, 1203–1206.